

Synthesis Characterization and Electrochemical Performance of Chromium Doped Tin Oxide

David Bahati^{1*}, Mukka Prasanna², Pulapa Venkata Kanaka Rao¹

¹University of Dodoma, Tanzania

²Centre for nano science and technology, India

*Corresponding author: Davic Bahati: david.bahati@udom.ac.tz



Citation: Bahati D., Prasanna M., Rao P.V.K. (2020) Synthesis Characterization and Electrochemical Performance of Chromium Doped Tin Oxide. Open Science Journal 5(3)

Received: 9th April 2020

Accepted: 15th June 2020

Published: 27th July 2020

Copyright: © 2020 This is an open access article under the terms of the [Creative Commons Attribution License](#), which permits unrestricted use, distribution, and reproduction in any medium, provided the original author and source are credited.

Funding: The author(s) received no specific funding for this work

Competing Interests: The author has declared that no competing interests exist.

Abstract:

Chromium doped Tin oxide nanoparticles with chromium concentrations ranging from 1 to 5 wt% were synthesized by microwave irradiation technique. Standard characterization techniques were used to understand the characteristics of the nanoparticles obtained. X-Ray Diffraction (XRD) pattern depicted the tetragonal crystal structure for Cr doped SnO₂ nanoparticles. From the results of crystallite sizes for various doping concentrations, it was observed that doping inhibits the growth of crystalline grains of SnO₂. Scanning Electron Microscope (SEM) images confirmed the surface morphology modifications due to varying doping concentration of Cr, nanocrystallite showed extra agglomerated status with mesoporous structures. Energy dispersive spectrometer (EDAX) observations confirmed the doping of chromium ions in SnO₂ lattice. Other standard characterization techniques such as FESEM, TEM, HRTEM, FTIR, UV-Vis spectroscopic analysis were also carried out for the samples prepared. The electrochemical behavior of the sample was determined using Cyclic Voltammetry (CV) by scanning the potential at a rate of 50 mV s⁻¹ and for a maximum current of 600 mA carried out on undoped SnO₂ and Cr doped SnO₂. It was observed that as the wt% of Cr in Cr doped SnO₂ increases, the electrochemical performance increases as compared to undoped SnO₂. A fairly larger peak current of 15 μ A and a larger oxidation peak potential of 0.76 V were observed for 5 wt% Cr doped SnO₂.

Keywords: Tin Oxide (SnO_2), Chromium(Cr), Microwave irradiation, XRD, FESEM, HRTEM, FTIR, UV-Vis spectroscopy and Cyclic voltammetry (CV).

Introduction

Nanostructured metal-oxide semiconductor based sensors have wide applications in biological, environmental and analytical chemistry (1–5). Among the oxide semiconductors, tin oxide (SnO_2) is one of the promising candidates as a host material that has been used in gas sensors, dye-sensitized solar cells, electrochromic windows, transparent conducting electrodes, transistors, catalysts and supercapacitors (6–10). SnO_2 is a versatile material with a wide band gap (3.6 eV at 300 K) in its stoichiometric form, but due to lattice imperfections and oxygen vacancies arising during its production, it becomes n-type and conductive (9,11–13). SnO_2 material research has been of considerable interest because of its combined properties of plentiful oxygen vacancies, high optical transparency, chemical and electrochemical stability, good electrocatalytic activity, nontoxicity, good biocompatibility, and high electron communication features when doped (14). Chemical doping with appropriate elements (Fe, Cr, Co, Mn, Ni, etc.) is widely used as an effective method to tune surface states, energy levels of semiconductors and transport performance of carriers which enhances the electrical, electrochemical and magnetic properties of materials (12,14). The ionic radius of Cr^{3+} is close to that of Sn^{4+} (15,16), which means that Cr^{3+} can easily penetrate into the SnO_2 crystal lattice or substitute the Sn^{4+} position in the crystal. Various methods have been used to synthesize the SnO_2 nanostructures; Autoclave method, co-precipitation, pulsed laser deposition, spray pyrolysis, solid state reaction method, polymeric precursor's route, hydrothermal method etc. (17–21). However, it still remains a great challenge to develop a simple method for fabricating nano- SnO_2 , particularly metal ion doped SnO_2 nanostructures with controlled morphology. Herein we report the synthesis of Cr doped SnO_2 nanoparticles by a simple microwave irradiation method that takes only a few minutes to complete the reaction with prevented agglomeration.

Experimental details

Materials

Chromium (III) nitrate nonahydrate [$\text{Cr}(\text{NO}_3)_3 \cdot 9\text{H}_2\text{O}$] and Stannous (II) Chloride dihydrate [$\text{SnCl}_2 \cdot 2\text{H}_2\text{O}$] from Fischer Scientific, were the starting materials used without further purification. Phosphate Buffer solution (PBS), Ammonium Hydroxide (NH_4OH) and ultrapure deionized water was used as solvent.

Nanoparticle synthesis

The growth solution of SnO₂ is prepared by dissolving 0.1M Stannous (II) Chloride dihydrate [SnCl₂·2H₂O] in deionized water, Ammonium hydroxide (NH₄OH) was added drop wise (about 1 drop per 3–4 s) to the above solution until the pH reached 10. This solution was again stirred for 30 minutes to form a greenish colloidal gel. Further, the hydroxide product was washed several times with deionised water and ethanol in order to remove the excess Cl⁻ and NH₄⁺ ions. Then the precipitate containing beaker was transferred into a microwave oven (600 W) and kept for 20 minutes. The product obtained is tin hydroxide which is calcinated at 800 °C for 4 hour to get the tin oxide nanoparticles. For doping approximate amounts of [Cr(NO₃)₃·9H₂O] with different Cr (1% , 3% and 5% by wt) content were mixed with Stannous (II) Chloride dihydrate [SnCl₂·2H₂O] in deionized water, Ammonium hydroxide (NH₄OH) was added drop wise until the pH reached 8 for all doping concentrations. Then the precipitate was washed with ethanol to remove excess Cl⁻ and NH₄⁺ ions and the beakers were transferred into microwave oven (600 W) and kept for 20 minutes. Finally, the Cr doped SnO₂ nanopowders were obtained after annealing the precipitates at 600 °C for 5 hours in an ambient atmosphere.

Results and discussions

XRD Analysis

Figure 1 shows the results of XRD analysis of the undoped SnO₂ and Cr doped SnO₂ Nanoparticles obtained using Microwave Method.

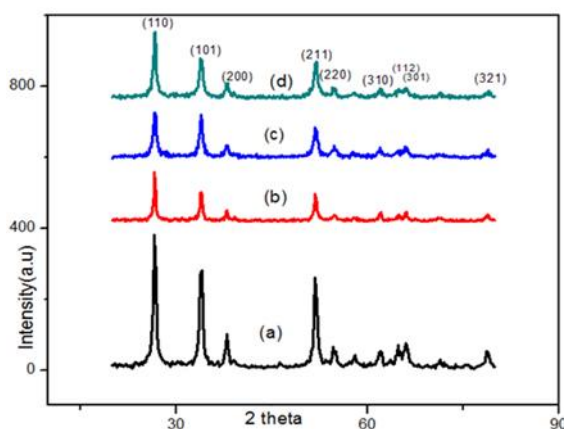


Figure.1: XRD patterns of (a) undoped SnO₂, (b) 1 wt%, (c) 3 wt%, and (d) 5 wt% Cr doped SnO₂ nanoparticles

The XRD patterns of undoped SnO₂ exhibit diffraction planes along (110), (101), (200), (211), (220), (310), (112), (301) and (321), which is consistent with rutile-type phase and tetragonal unit cell of SnO₂ (ICDD-PDF card no.46-0255). From figure 1 it is observed that there is increase in the peak intensities for Cr doped SnO₂ with no extra phase as the Cr concentration increases and is depicted that chromium ions substitute tin ions in tin oxide lattice. The observed

shrinkage of the unit cell volume is consistent with the fact that the ionic radius and valence of Cr^{3+} (63 °Å) is smaller than that of Sn^{4+} (74 °Å). The XRD results showed that the Cr^{3+} ions incorporate into SnO_2 lattice or replace Sn^{4+} sites without changing the rutile structure. The average crystallite size (D) was determined using the diffraction peaks of (110) and (101) from Scherer's formula

$$D = \frac{K\lambda}{\beta \cos\theta} \quad (1)$$

(22,23). Where K is the shape factor whose value is taken as 0.89, λ is the wavelength of Cu Ka radiation, and β is the corrected full width at half maximum (FWHM) of the diffraction peak and θ is the diffracting angle. The average crystallite sizes of the synthesized nanoparticles were 17.88 nm (undoped), 26.41 nm (1% by wt), 28.50 nm (3% by wt) and 49.46 nm (5% by wt) respectively. These results indicate that the crystallite size of the Cr doped SnO_2 nanoparticles increase as the doping concentration increases.

Scanning electron microscopy (SEM) analysis

Figure 2 shows the SEM images of undoped and Chromium doped SnO_2 . It is observed that the prepared SnO_2 particles are nanorods with some agglomeration, which may be due to annealing of SnO_2 nanoparticles (NPs). However there is some non-uniformity in the shape and the existence of porosity. The measured mean particle size of the tin dioxide particles from the SEM image is 47.8 nm, which is comparable to XRD values determined for the particle size. A relatively uniform mixture of tetragonal like structures could be observed and the nanocrystallite showed extra agglomerated status with mesoporous structures.

Elemental analysis of NPs was done by using energy dispersive spectrometer (EDS) the plot of spectrum is shown in Figure 4. Emission peaks such as O and Sn observed in the EDS spectrum shows the presence of tin and oxygen elements and confirmed the stoichiometry of NPs.

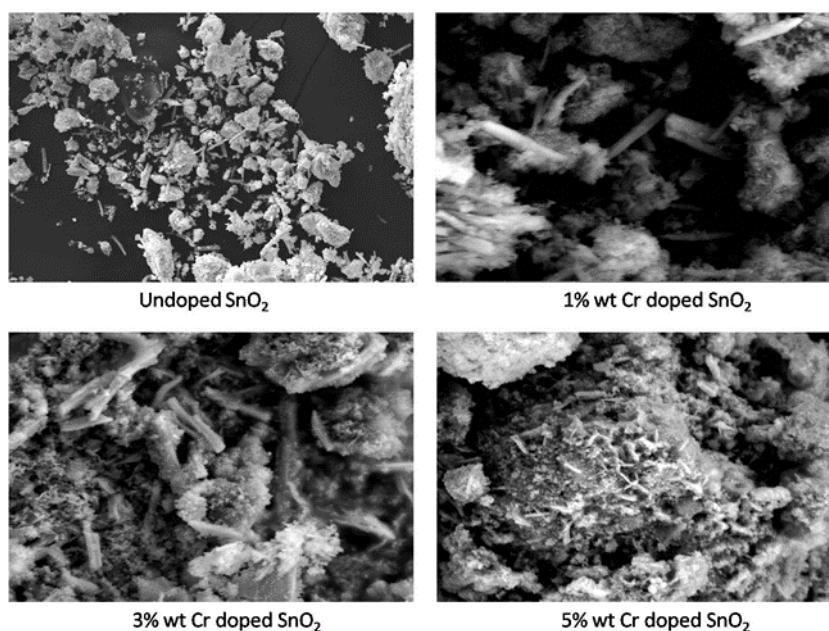


Figure. 2: SEM images for undoped and Cr-doped Tin Oxide

Field emission scanning electron microscopy (FESEM) analysis

Field Emission Scanning Electron Microscope (FESEM) was used to observe the morphology and structure changes. Figure 3 show that doping significantly alters the morphology of the nanorods. The surface of the SnO₂ particles with 1% Cr doping are nano rods as shown in Figure 3(a), the grain size formed and surface modifications by increasing the concentration to 3 wt% is shown in Figure 3(b), modification of surface are also evident on increasing the Cr dopant level to 5 wt%, it is observed that the grain size formed on the surface of SnO₂ film decreases on increase of Cr dopant (Figure 3(c)). Further large regular rectangular and triangular shaped grains are formed on the surface of SnO₂ and the size of grains decrease with increasing dopant concentration.

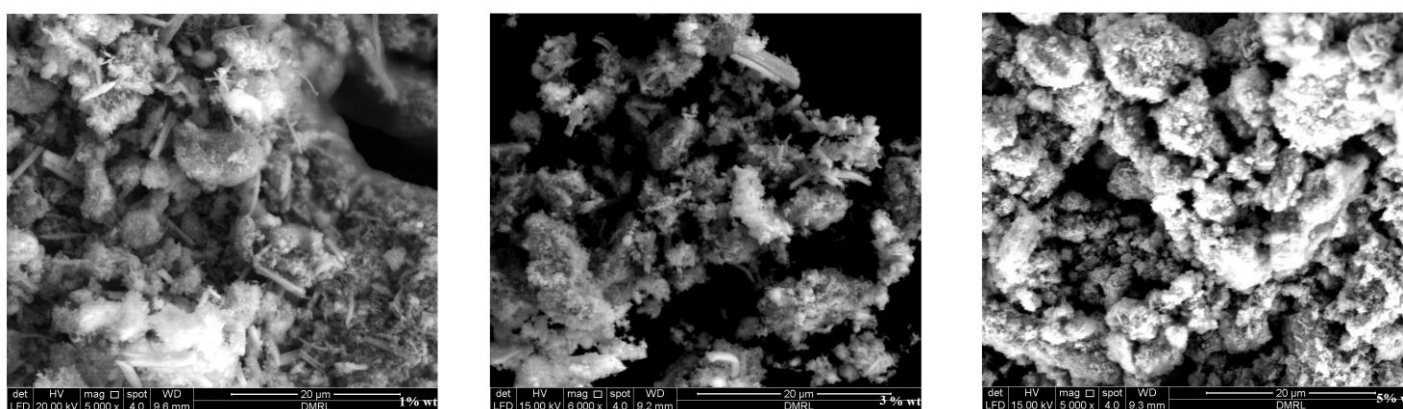


Figure. 3: FESEM Images of (a) 1wt% (b) 3 wt% and (c) 5 Wt% Cr doped SnO₂

Energy dispersive analysis of X-Ray (EDAX)

Figure 4 shows the compositional analyses of the Cr doped samples as depicted in the EDX spectra. The spectra show chromium peaks implying incorporation of Cr ions into SnO₂ lattice. Furthermore, Hume-Rothery rules of substitutional solid solution suggest that substitutional incorporation of dopant is possible if the ionic radii of the host atom and the dopant must not differ by more than 5% (24–26). In this investigation, the ionic radii of Sn⁴⁺ and Cr³⁺ are 0.069 and 0.063 nm, respectively, which are well within 5% difference. This shows that Cr ions substitutionally replace Sn ions in the SnO₂ lattice.

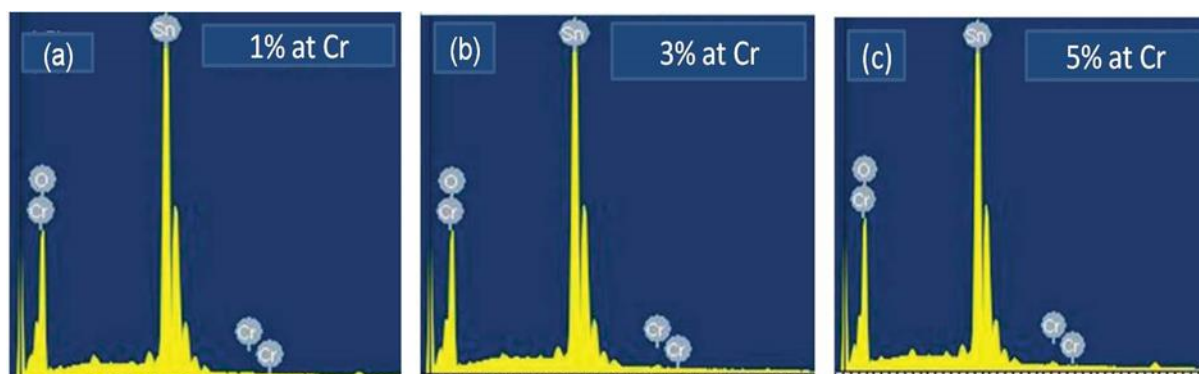


Figure 4: EDAX spectra of (a) 1 wt% (b) 3 wt% and (c) 5 Wt% Cr doped SnO₂

Fourier transform infrared (FTIR) spectroscopy

FTIR analysis is carried out in the wavenumber range from 450 cm^{-1} to 4000 cm^{-1} . The samples are with KBr, thoroughly mixed and pelletized by pressing under sufficient pressure, before FTIR analysis. FTIR spectra of SnO_2 nanoparticles prepared at 600 $^\circ\text{C}$ are shown in Figure 5. The broad peak centered at 619 cm^{-1} is observed. The broad band between 800 and 500 cm^{-1} was due to the vibrations of Sn-O. To obtain more details of defects in $\text{SnO}_2\text{:Cr}$ films FTIR is employed. The main IR features of SnO_2 at 468 and 619 cm^{-1} are assigned to O-Sn-O and Sn-O stretching vibrations, respectively. Two interesting features are observed: One is the weak feature of O-Sn-O vibration in the undoped SnO_2 film, which goes with the presence of vibration at 644 cm^{-1} . This vibration becomes weakened and disappears as the Chromium (Cr) concentration increases; the other characteristic is the presence of Sn-Cr feature at high doping levels, which causes the splitting of O-Sn-O feature. A band corresponding to the presence of adsorbed water (H_2O) 1630~1640 cm^{-1} and hydroxide absorption (OH) bands in the range of 2500~3500 cm^{-1} were observed.

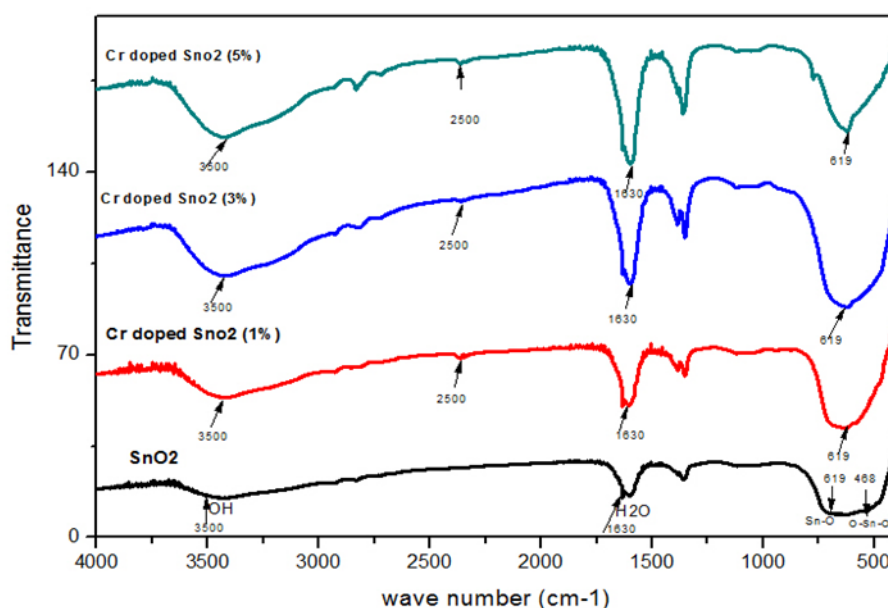


Figure 5: FTIR spectra of undoped SnO_2 and Cr doped SnO_2

Transmission electron microscope (TEM) analysis

Typical TEM and high-resolution transmission electron microscope (HRTEM) images of undoped and 5 wt% Cr doped SnO_2 samples are shown in Figure 6 (a & c) a spherical morphology with average size of 21nm and 16 nm respectively is observed the results are in good agreement with the estimated average crystallites size from the XRD pattern. The HRTEM image for undoped and 5 wt% Cr doped SnO_2 nanoparticles are shown in Figure 6 (b & d). Undoped SnO_2 nanocrystallites exhibited highly symmetrical and sharp lattice lines which confirm their single crystalline and defect free nature. However, Cr-doping seems to introduce twin-like defects in the crystallites as shown in Figure 6(d). Further,

presence of any secondary phase or trace elements in the samples is not identified using HRTEM.

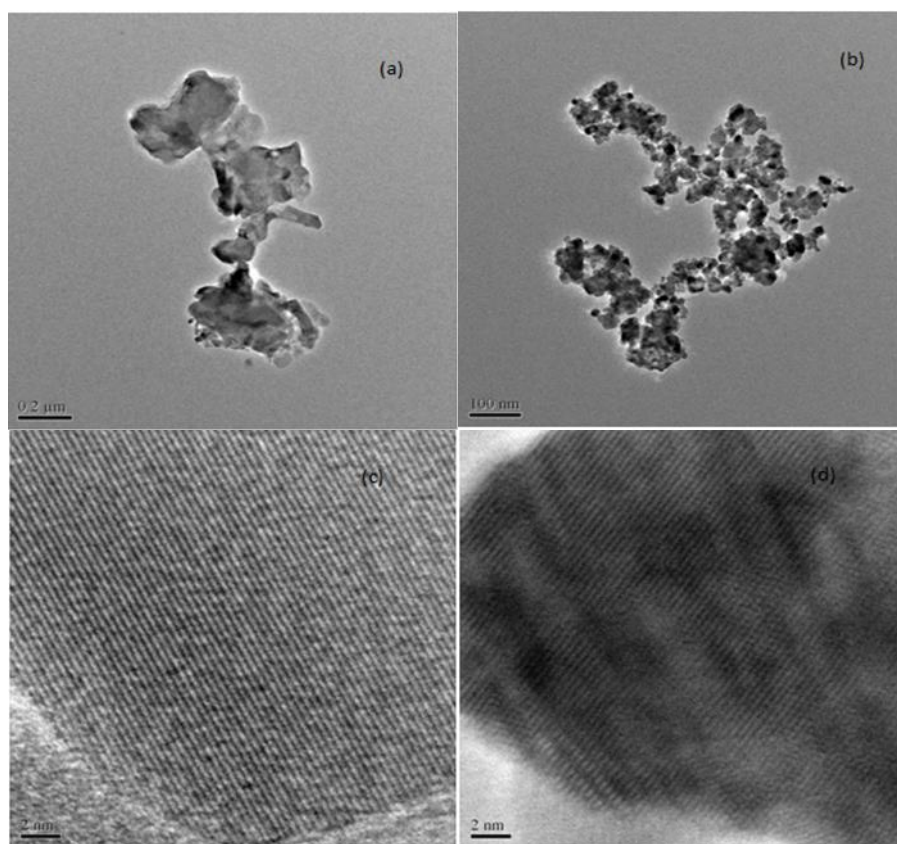


Figure 6: TEM image of (a) undoped SnO_2 , (c) 5 wt% Cr doped SnO_2 nanoparticles & HRTEM images of (b) undoped SnO_2 , (d) 5 wt% Cr doped SnO_2 nanoparticles

Optical band-gap using UV-Visible spectrophotometer

From the transmittance spectra shown in Figure 7 the Optical band gap values were obtained using the Tauc's formula (27). For undoped SnO_2 band gap is 3.58 eV which is in good agreement with the reported values of Arun kumar sinha (11) it is observed that Cr doping has a positive influence on the temperature dependent of resistance.

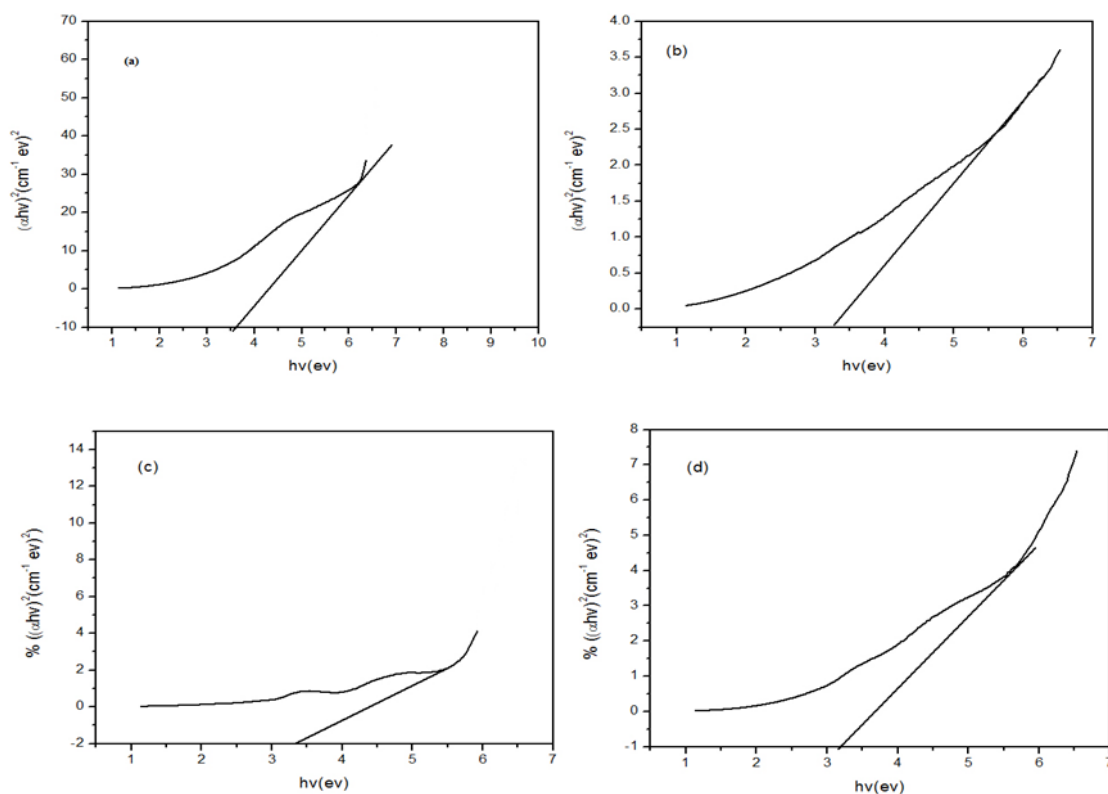


Figure 7: Band gap energy of (a) undoped SnO₂, (b) 1 wt% (c) 3 wt% and (d) 5 wt% Cr doped SnO₂ nanoparticles

Cyclic voltammetry analysis

The electrochemical behaviour of the sample is determined using Cyclic Voltammetry (CV) by scanning the potential at a rate of 50 mV s⁻¹ and for a maximum current of 600mA carried out on undoped SnO₂ and Cr doped SnO₂. From figure 8 it is observed that for undoped SnO₂ (Figure 8(a)) the peak current is 11 μ A for doping concentration of 1wt % the peak current is 12 μ A for doping concentration of 3 wt% the peak current is 13 μ A, as the wt% of Cr in Cr doped SnO₂ increases, the electrochemical performance increases as compared to undoped SnO₂, a fairly larger peak current of 15 μ A and a larger oxidation peak potential of 0.76 V were observed for 5 wt% Cr doped SnO₂.

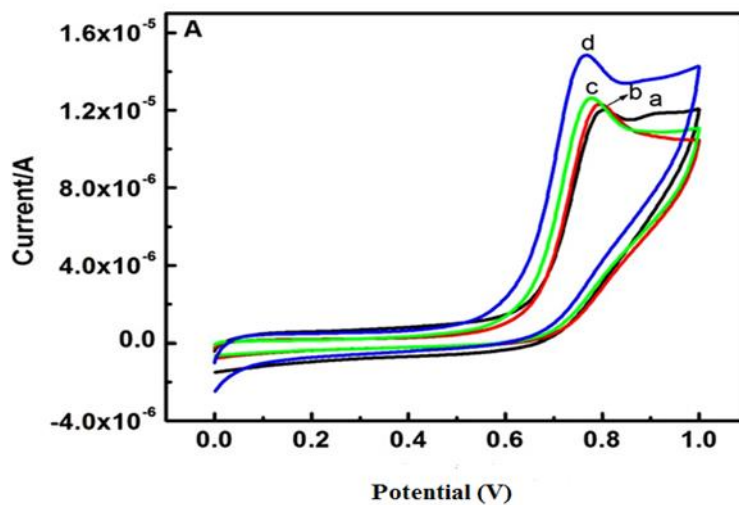


Figure 8: Cyclic Voltammetry of (a) undoped SnO₂, (b) 1 wt% doped (c) 3 wt% doped and (d) 5 wt% Cr-doped SnO₂ nanoparticles

Conclusion

Undoped and Cr doped SnO₂ nanoparticles were synthesised using microwave irradiation method. The influence of Cr doping concentration on the structure, morphology, optical and electrochemical properties are reported. XRD patterns of undoped sample revealed the pure tetragonal rutile structure of SnO₂. UV Spectroscopy shows decreasing band gap of SnO₂ by addition of Chromium. The cyclic voltammetric (CV) studied confirmed that Cr doped sample have good electrochemical behaviour when compare to pure SnO₂ sample.

References:

1. Penner RM. Chemical Sensing with Nanowires. *Annu Rev Anal Chem.* 2012 Jul 19;5(1):461–85.
2. Kolmakov A, Moskovits M. Chemical Sensing and Catalysis by One-Dimensional Metal-Oxide Nanostructures. *Annu Rev Mater Res* [Internet]. 2004 Aug 4 [cited 2019 Dec 10];34(1):151–80. Available from: <http://www.annualreviews.org/doi/10.1146/annurev.matsci.34.040203.112141>
3. Devan RS, Patil RA, Lin J-H, Ma Y-R. One-Dimensional Metal-Oxide Nanostructures: Recent Developments in Synthesis, Characterization, and Applications. *Adv Funct Mater* [Internet]. 2012 Aug 21 [cited 2019 Dec 10];22(16):3326–70. Available from: <http://doi.wiley.com/10.1002/adfm.201201008>
4. Afzal A, Cioffi N, Sabbatini L, Torsi L. NO_x sensors based on semiconducting metal oxide nanostructures: Progress and perspectives. Vols. 171–172, *Sensors and Actuators, B: Chemical*. 2012. p. 25–42.
5. Ibupoto ZH, Shah SMUA, Khun K, Willander M. Electrochemical L-Lactic Acid Sensor Based on Immobilized ZnO Nanorods with Lactate Oxidase. *Sensors* [Internet]. 2012 Feb 23 [cited 2019 Dec 10];12(3):2456–66. Available from: <http://www.mdpi.com/1424-8220/12/3/2456>
6. Sun C, Mathews N, Zheng M, Sow CH, Wong LH, Mhaisalkar SG. Aligned Tin Oxide Nanonets for High-Performance Transistors. *J Phys Chem C* [Internet]. 2010 Jan 21 [cited 2019 Dec 10];114(2):1331–6. Available from: <https://pubs.acs.org/doi/10.1021/jp909673j>
7. Al-Janaby AZ, Al-Jumaili HS. Structural, Optical and Sensitive Properties of Ag-Doped Tin Oxide Thin Films [Internet]. *International Research Journal of Engineering and Technology*. 2016 [cited 2019 Dec 10]. Available from: www.irjet.net
8. Tazikheh S, Akbari A, Talebi A, Talebi E. Synthesis and characterization of tin oxide nanoparticles via the Co-precipitation method. *Mater Sci* [Internet]. 2014 [cited 2019 Dec 10];32(1):98–101. Available from: <http://www.materialsscience.pwr.wroc.pl/>

9. Werner J, Walter A, Rucavado E, Moon SJ, Sacchetto D, Rienaecker M, et al. Zinc tin oxide as high-temperature stable recombination layer for mesoscopic perovskite/silicon monolithic tandem solar cells. *Appl Phys Lett*. 2016 Dec 5;109(23).
10. Kou L, Li C, Zhang Z, Guo W. Electric-field- and hydrogen-passivation-induced band modulations in armchair ZnO nanoribbons. *J Phys Chem C*. 2010 Jan 21;114(2):1326–30.
11. Sinha AK, Manna PK, Pradhan M, Mondal C, Yusuf SM, Pal T. Tin oxide with a p-n heterojunction ensures both UV and visible light photocatalytic activity. *RSC Adv*. 2014;4(1):208–11.
12. Venugopal B, Nandan B, Ayyachamy A, Balaji V, Amirthapandian S, Panigrahi BK, et al. Influence of manganese ions in the band gap of tin oxide nanoparticles: Structure, microstructure and optical studies. *RSC Adv*. 2014;4(12):6141–50.
13. Banyamin Z, Kelly P, West G, Boardman J. Electrical and Optical Properties of Fluorine Doped Tin Oxide Thin Films Prepared by Magnetron Sputtering. *Coatings [Internet]*. 2014 Oct 30 [cited 2019 Dec 12];4(4):732–46. Available from: <http://www.mdpi.com/2079-6412/4/4/732>
14. Agrahari V, Mathpal MC, Kumar S, Kumar M, Agarwal A. Cr modified Raman, optical band gap and magnetic properties of SnO₂ nanoparticles. *J Mater Sci Mater Electron*. 2016 Jun 1;27(6):6020–9.
15. Tandon B, Yadav A, Khurana D, Reddy P, Santra PK, Nag A. Size-Induced Enhancement of Carrier Density, LSPR Quality Factor, and Carrier Mobility in Cr–Sn Doped In₂O₃ Nanocrystals. *Chem Mater [Internet]*. 2017 Nov 14 [cited 2019 Dec 12];29(21):9360–8. Available from: <https://pubs.acs.org/doi/10.1021/acs.chemmater.7b03351>
16. Subramanyam K, Sreelekha N, Murali G, Reddy DA, Vijayalakshmi RP. Structural, optical and magnetic properties of Cr doped SnO₂ nanoparticles stabilized with polyethylene glycol. *Phys B Condens Matter*. 2014 Dec 1;454:86–92.
17. Anandan K, Rajendran V. Size Controlled Synthesis Of SnO₂ Nanoparticles: Facile Solvothermal Process. Vol. 2, *Journal of Non-Oxide Glasses*. 2010.
18. Krishna M, Komarneni S. Conventional- vs microwave-hydrothermal synthesis of tin oxide, SnO₂ nanoparticles. *Ceram Int*. 2009 Dec;35(8):3375–9.
19. Lim SP, Huang NM, Lim HN. Solvothermal synthesis of SnO₂/graphene nanocomposites for supercapacitor application. *Ceram Int*. 2013 Aug;39(6):6647–55.
20. Kim HW, Na HG, Kwon YJ, Kang SY, Choi MS, Bang JH, et al. Microwave-Assisted Synthesis of Graphene-SnO₂ Nanocomposites and Their Applications in Gas Sensors. *ACS Appl Mater Interfaces*. 2017 Sep 20;9(37):31667–82.
21. Zhong C, Wang J, Chen Z, Liu H. SnO₂ –Graphene Composite Synthesized via an Ultrafast and Environmentally Friendly Microwave Autoclave Method and Its Use as a Superior Anode for Lithium-Ion Batteries. *J Phys Chem C [Internet]*. 2011 Dec 22 [cited 2019 Dec 13];115(50):25115–20. Available from: <https://pubs.acs.org/doi/10.1021/jp2061128>
22. Kishore Kumar YB, Suresh Babu G, Uday Bhaskar P, Sundara Raja V. Preparation and characterization of spray-deposited Cu₂ZnSnS₄ thin films. *Sol Energy Mater Sol Cells*. 2009 Aug;93(8):1230–7.
23. Azam A, Ahmed F, Arshi N, Chaman M, Naqvi AH. Formation and characterization of ZnO nanopowder synthesized by sol-gel method. *J Alloys Compd*. 2010 Apr 30;496(1–2):399–402.
24. Zhu L, Wang H, Wang Y, Lv J, Ma Y, Cui Q, et al. Substitutional alloy of Bi and Te at high pressure. *Phys Rev Lett*. 2011 Apr 8;106(14).
25. Ren MX, Li BS, Fu HZ. Formation condition of solid solution type high-entropy alloy. *Trans Nonferrous Met Soc China (English Ed)*. 2013 Apr;23(4):991–5.
26. Wang Z, Huang Y, Yang Y, Wang J, Liu CT. Atomic-size effect and solid solubility of multicomponent alloys. *Scr Mater*. 2015 Jan 1;94:28–31.
27. Chrysicopoulou P, Davazoglou D, Trapalis C, Kordas G. Optical properties of very thin (< 100 nm) sol-gel TiO₂ films. *Thin Solid Films*. 1998 Jun 22;323(1–2):188–93.